THE JOURNAL OF PHYSICAL CHEMISTRY C
A JOURNAL OF THE AMERICAN CHEMICAL SOCIETY

pubs.acs.org/JPCC

Article

Nonlocal Interactions in the Double Perovskite Sr_2FeMoO_6 from Core-Level X-ray Spectroscopy

Published as part of The Journal of Physical Chemistry virtual special issue "D. D. Sarma Festschrift".

Dibya Phuyal,* Soham Mukherjee, Swarup K. Panda, Gabriel J. Man, Konstantin Simonov, Laura Simonelli, Sergei M. Butorin, Håkan Rensmo, and Olof Karis*

Cite This: *J. Phys. Chem. C* 2021, 125, 11249−11256

Read Online

ACCESS | Metrics & More | Article Recommendations | Supporting Information

ABSTRACT: The valence electronic structure of the half-metallic double perovskite Sr_2FeMoO_6 forms from a strongly hybridized band in the spin-down channel of Fe 3d and Mo 4d states that provides metallic conductivity and a gapped spin-up channel. The ground-state description has previously been explored in terms of many-body interactions where local and nonlocal interactions produce states with a combination of a charge-transfer configuration and intersite charge fluctuations. Here, we provide a qualitative understanding on nonlocal effects in Sr_2FeMoO_6 using a combination of core-level X-ray spectroscopies, specifically X-ray absorption, emission, and photoelectron spectroscopies. Our spectroscopic data indicate intersite Fe 4p−O 2p−Mo 4d interactions to be the origin of these nonlocalized transitions. Close to the Fermi level, this interaction is dominated by Mo 4d−O 2p character. When our data are compared against first-principles electronic structure calculations, we conclude that a full understanding of the nature of these states requires a spin-resolved description of the hybridization functions and that the nonlocal screening occurs predominantly through hybridization in the minority spin channel of the Mo 4d bands.

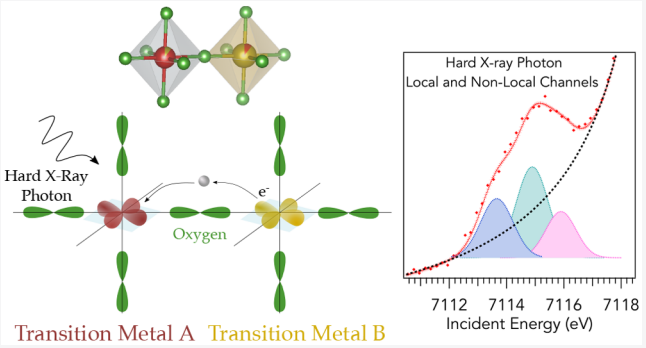

INTRODUCTION

Double perovskite (DP) oxides offer a unique material framework to engineer a wide range of physics with a multitude of functionalities. In its simplest form, the DP structure ($A_2BB'O_6$) consists of two transition metal (TM) ions interspersed by corner-sharing octahedra that can be arranged in a rock-salt, layered, or columnar order.[1] This means that this type of perovskite oxide can accommodate a range of suitable A- and B-type cations, altering its microscopic interactions and, in turn, dramatically affecting a material's macroscopic properties. More specifically, the choice of the B/B′ cations can profoundly alter a material's electronic structure, creating materials with desired functionalities ranging from spin-polarized metals to strongly correlated systems, spin−orbit effects, ferroelectricity, and complex magnetic properties, to name a few examples.[2−7]

The proximity effects of two separated octahedra of B cations in DP oxides with varying ionic size and valence states produce materials with different structural and electronic characteristics. The electronic and magnetic properties are governed by the spatially extended TM d orbitals and therefore by the balance between bandwidth, crystal-field splitting of the d orbitals, electron−electron correlations, and spin−orbit coupling in 4d/5d elements, making the prediction of DP's properties complex.[1] The interaction between neighboring metal components is simultaneously active and has encouraged research to uncover new fundamental properties as well as materials with properties that can be engineered for use in a range of applications from spintronics to catalysis.[8]

One of the most studied materials in this class is the half-metallic and ferrimagnetic Sr_2FeMoO_6 (henceforth termed SFMO).[9] It is known to have a purely spin-polarized band structure where only one-spin direction is present at the Fermi level.[9−11] The large room-temperature magnetoresistance is noteworthy for its potential use in spintronic devices based on the high spin polarization of charge carriers.[7,12−15] In the ionic picture, the electronic structure is understood to have a $Fe^{3+}(3d^5)$ sites as localized with a high-spin $S = 5/2$ configuration together with $Mo^{5+}(4d^1)$ sites with one

Received: March 22, 2021
Revised: May 1, 2021
Published: May 13, 2021

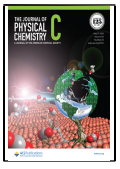

conduction electron that can hop between Mo and Fe sites in the exchange split t_{2g} orbitals.[16−18] The complete ground-state electronic structure description in SFMO presents a more complex picture due to the large Fe−O and Mo−O hybridization as well as the importance of nonlocal Fe−O−Mo charge fluctuations.[19,20] This intricacy arises from the antiferromagnetic coupling between Fe and Mo sites, e.g., unlike the ferromagnetic coupling in manganites. In contrast to manganites like $La_{1-x}Sr_xMnO_3$, the strong local coupling in SFMO only applies to every other site since Mo is paramagnetic.[19] Unlike most common half-metals such as Heuslers or manganites, SFMO has a large localized moment associated with the Fe 3d shell and antiparallel moment associated Mo 4d states. Thus, an antiferromagnetic (AFM) exchange interaction results between Fe localized moments and conduction electrons. This relationship of interatomic electronic and magnetic structures and competition between electron localization and hybridization are relevant ingredients in determining a material's Curie temperature and ferromagnetic state.[15] This nonlocal interaction between every other Fe site produces interesting coupling schemes that constitute the basis of this study and relevant to other magnetic perovskite oxides.

In this article, we provide a detailed view of the local and nonlocal Fe energy levels of Sr_2FeMoO_6 comparison to several Fe-based oxides to show how nonlocal effects are important to understand this material. Core-level X-ray spectroscopic methods are extensively used for studying 3d electrons and their local and nonlocal effects.[21] Nonlocal effects, sensitive to aspects of intersite interactions, leave signatures in the X-ray absorption, emission, and photoemission spectra. Here, we employ Fe K-edge X-ray absorption (XAS) and X-ray emission spectroscopy (XES) to gain valuable information about the spin density of Sr_2FeMoO_6 and use a partial fluorescence absorption spectrum to reveal features related to this intersite hybridization. The pre-edges region of a K-edge XAS is typically comprised of relatively low-intensity structures due to weak 1s → 3d quadrupole transitions. For Sr_2FeMoO_6, this feature has larger intensity when compared with other similar oxide perovskites where Fe^{3+} remains octahedrally coordinated by O_2^- ions. We furthermore find that hard X-ray photoemission spectroscopy (HAXPES) for the Fe 2p core-level spectra show structures characteristic of nonlocal screening channels. Calculations from local density approximation (LDA) with density functional theory (DFT) can explain these features by examining the hybridization potential function which can be used to investigate the amount and intensity of hybridized Fe 3d−O 2p−Mo 4d states, especially near the Fermi level.

EXPERIMENTAL SECTION

Polycrystalline Sr_2FeMoO_6, α-Fe_2O_3, and $LaFeO_3$ pellets were prepared by conventional solid-state synthesis as described in ref 22. $SrCO_3$ is preheated at 150 °C to remove any absorbed water. The stoichiometric mixture of highly pure $SrCO_3$, α-Fe_2O_3, and MoO_3 is first heated at 900 °C for 12 h for calcination. The obtained powder is then annealed to 1500 °C in a reducing atmosphere 98% Ar/2% H_2 gas for 12 h. The powder was finally pressed to 5 GPa to form a 5 mm diameter pellet and subsequently sintered for 6 h at 1500 °C. Polycrystalline Ca_2FeReO_6 was prepared by solid-state reaction as previously reported.[23] The phase purity and ordering were checked by laboratory X-ray diffraction (PANanalytical MRD II). The X-ray diffraction pattern was indexed with the (111) and (311) Bragg peaks that are due to the alternating order of the Fe and Mo sites. The sample is highly ordered, and no impurity peaks are found in the XRD pattern.

X-ray absorption and emission measurements at the Fe K-edge edge were performed at the CLÆSS beamline[24] of the ALBA Synchrotron (Barcelona, Spain) using a Si (311) double-crystal monochromator. The spectra were recorded by monitoring the emission of the $K\beta_{1,3}$ (≈ 7058 eV) or $K\beta'$ (≈ 7045 eV) emission lines and scanning the incoming energy across the Fe K-edge absorption edge. The Fe fluorescence energy was selected by using a Si (333) dynamical bent diced analyzer crystal and an energy dispersive one-dimensional (1D) detector in Rowland circle geometry (Rowland radius = 1 m). The overall energy resolution was determined to 0.8 eV from the full width at half-maximum (fwhm) of the quasi-elastic peak collected from a Kapton tape. The spectrometer energy window around the Fe $K\beta_{1,3}$ emission line window was 15 eV. Spin-selective high-resolution fluorescence detected X-ray absorption (HERFD-XANES) was acquired by selecting $K\beta_{1,3}$ and $K\beta'$ fluorescence lines, which correspond to final states with the unpaired spin in the 3p shell either parallel or antiparallel to the unpaired spin in the 3d shell.[25] Our fitting procedure is applied in the range 7110−7119 eV with Gaussian peaks whose widths are constrained to the experimental resolution. The background was fitted by using an arc-tangent function having a fwhm of ∼1.8 eV and a centroid energy of ∼7120 eV to account for the leading edge of the intense dipolar transition. Oxygen K-edge XAS were measured at the 8.0.1 beamline[26] at the Advanced Light Source (Berkeley, CA). The X-ray absorption spectrum was acquired in both total electron yield (TEY) and total fluorescence yield (TFY) modes at room temperature and under a high vacuum of 10^{-10} mbar. Spectra obtained by TEY and TFY were qualitatively similar. Oxygen K-edge XAS data were calibrated by using the offset determined from the TiO_2 O K-edge.

Hard X-ray photoelectron spectroscopy measurements were performed at the P22 beamline[27] of the PETRA-III synchrotron in Hamburg, Germany. The incident photon energy was set to 4750 eV. The Fermi level was calibrated by using a clean Au foil in contact with the sample holder. The overall instrumental resolution was set to 300 meV. The photoelectrons were collected by using a SPECS 225 HV hemispherical analyzer at a near normal emission geometry with the incident X-ray at a 15° angle to the sample. The pressure in the main chamber was $\sim 10^{-10}$ mbar, and measurements were carried at room temperature (300 K).

COMPUTATION DETAILS

The density functional theory (DFT) calculations are performed in the generalized gradient approximation + Hubbard U (GGA+U) approach by means of a full potential linearized muffin-tin orbital method (FP-LMTO)[28,29] as implemented in the RSPt code.[30] The Brillouin-zone (BZ) integration is performed by using the thermal smearing method with 10 × 10 × 10 k-mesh which corresponds to 144 k-points in the irreducible part of the BZ. For the charge density and potential angular decomposition inside the MT spheres, the value of maximum angular momentum was taken equal to $l_{max} = 8$. To describe the electron−electron correlation within the GGA+U approach, we have used $U = 3$ eV and $J = 0.8$ eV for Fe d states. We note that our choice of U is guided by the recent study where such values of correlation

https://doi.org/10.1021/acs.jpcc.1c02580
J. Phys. Chem. C 2021, 125, 11249−11256

parameters were used to study SFMO in the GGA+U framework.[31]

After self-consistency is achieved, we used the spin-polarized GGA+U solution to compute the energy-dependent hybridization function $\Delta(E)$ of Mo and Fe d orbitals. If G_0 is the site projected Green's function obtained from DFT and H is the hybridization-free impurity Hamiltonian, with the corresponding energy E^{QI}, one obtains the following form of the hybridization function, $\Delta(E)$, via the Dyson equation:

$$G_0^{-1} = (E - E^{QI}) - \Delta(E)$$

The preceding expression is used to compute the hybridization function from our converged DFT calculations. In a quantum impurity model, $\Delta(E)$ gives the properties of the bath surrounding the impurity cluster and thus describes the interaction of an impurity electron (in our case, d-electrons of either Fe or Mo ions) with the bath consisting of all other electrons.

RESULTS AND DISCUSSION

The spin sensitivity in Kβ XES (3p → 1s) stems from the exchange coupling between unpaired 3p and unpaired 3d electrons. Via this coupling, the XES process provides an indirect probe of the local magnetic moment at the Fe 3d site and is therefore sensitive to the Fe spin state.[32,33] Figure 1 shows the Kβ XES spectrum taken at an incident energy of 7300 eV, far above the Fe K-edge absorption threshold. As mentioned above, the splitting of the Kβ into the K$\beta_{1,3}$ line and Kβ' originates from an exchange coupling between electrons in the 3d shells and a hole in the 3p shell. As is now established, the Kβ spectral shape and intensity are sensitive to the local spin state of the Fe ion and is more quantitatively estimated by comparing with references through the integral absolute difference (IAD) method.[34,35] From our IAD calculations, Sr_2FeMoO_6 shows a high-spin S = 2.5, an assignment similar to that of hematite (α-Fe_2O_3, S = 2.5) and $LaFeO_3$ (S = 2.5). Fe in both SFMO and $LaFeO_3$ systems resulted in a high-spin configuration, with five unpaired electrons occupying the 3d levels. The inset shows the relative variation of determined magnetic moment and IAD values plotted as a function of references and SFMO, where qualitatively similar trends are observed. We see that IAD depends linearly formal Fe valence and tracks with the experimental magnetic moment.

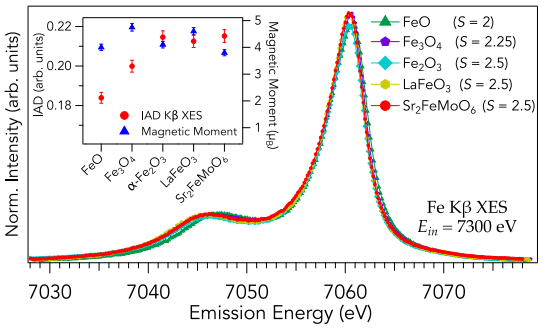

Figure 1. Normalized Fe Kβ XES of Sr_2FeMoO_6 and well-defined Fe spin systems measured at room temperature. The nominal spin density S is quantitatively derived from IAD analysis and plotted against formal spin and experimental determined magnetic moment (inset). The spectra are normalized to the integrated area.

One can separate the Kβ X-ray emission spectrum into an internally referenced spin-up and spin-down channels to obtain a local-spin selectivity in the K-edge absorption spectrum.[36−38] This is based on measuring partial fluorescence absorption spectrum by setting the emission energy selectively to either K$\beta_{1,3}$ or Kβ' satellite lines that are sensitive to the local 3d moment.[25] The K$\beta_{1,3}$ emission line leaves the final state with a spin-down reference in the 3p state, and Kβ' with a final state with a spin-up 3p state, as shown schematically in Figure 2a. Figure 2b shows the pre-edge region for spin-selective XANES spectra measured for K$\beta_{1,3}$ (spin-down) and Kβ' (spin-up) lines for SFMO; the inset shows the full energy range. Figure 2b clearly shows a distinct pre-edge feature for the spin-down channel that is absent for the spin-up channel. This is a direct consequence of the high-spin configuration of SFMO $3d^5$ (S = 2.5) as determined from our Kβ XES analysis discussed previously. Therefore, we expect only spin-down intermediate states to be available in the 1s → 3d transitions. This interpretation shows evidence for a purely spin-down band in SFMO's ground-state electronic structure.

The Fe K-edge 1s → 3p resonant X-ray emission (RXES) map for SFMO and related Fe^{3+} oxides is measured as the incident energy and emitted energy are varied, yielding a two-dimensional spectral surface as shown in Figure 3. The diagonal cut in a RXES map corresponds to the so-called high energy resolution fluorescence detection (HERFD) spectrum recorded as a partial fluorescence yield. In Figure 4a, we show HERFD spectra for SFMO and reference Fe^{3+} oxides, obtained at the K$\beta_{1,3}$ emission line. The partial yield spectrum shows better resolved spectral features compared to Fe K-edge conventional XANES,[39] particularly in the pre- and near-edge range. The absorption spectrum is referenced against FeO

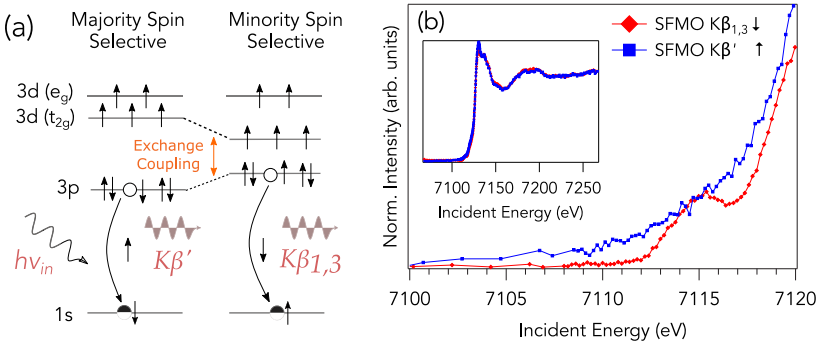

Figure 2. (a) Schematic representation of the two final state emission process in the atomic picture for Fe^{3+}. (b) HERFD-XANES taken at the maximum of spin-down selective K$\beta_{1,3}$ HERFD and spin-up Kβ' HERDF spectra.

https://doi.org/10.1021/acs.jpcc.1c02580
J. Phys. Chem. C 2021, 125, 11249−11256

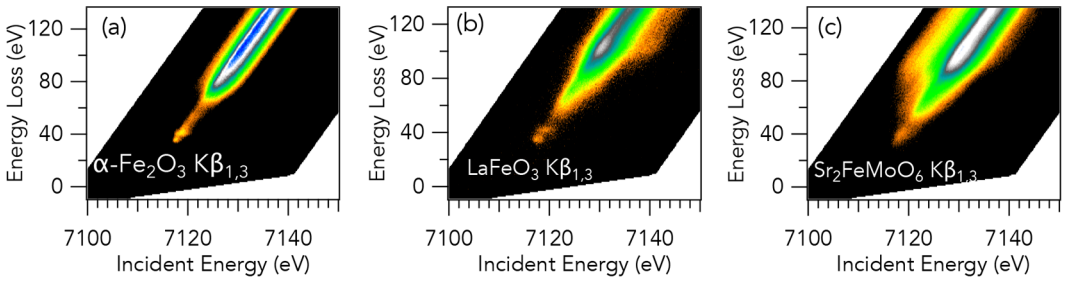

Figure 3. Fe K-edge 1s3p RXES map for (a) α-Fe_2O_3, (b) $LaFeO_3$, and (c) Sr_2FeMoO_6 measured at the maximum of the K$\beta_{1,3}$ emission line. The map is presented on an energy loss scale. A diagonal line, i.e., with unit slope, corresponds to a constant energy transfer where a HERFD-XANES spectrum can be extracted.

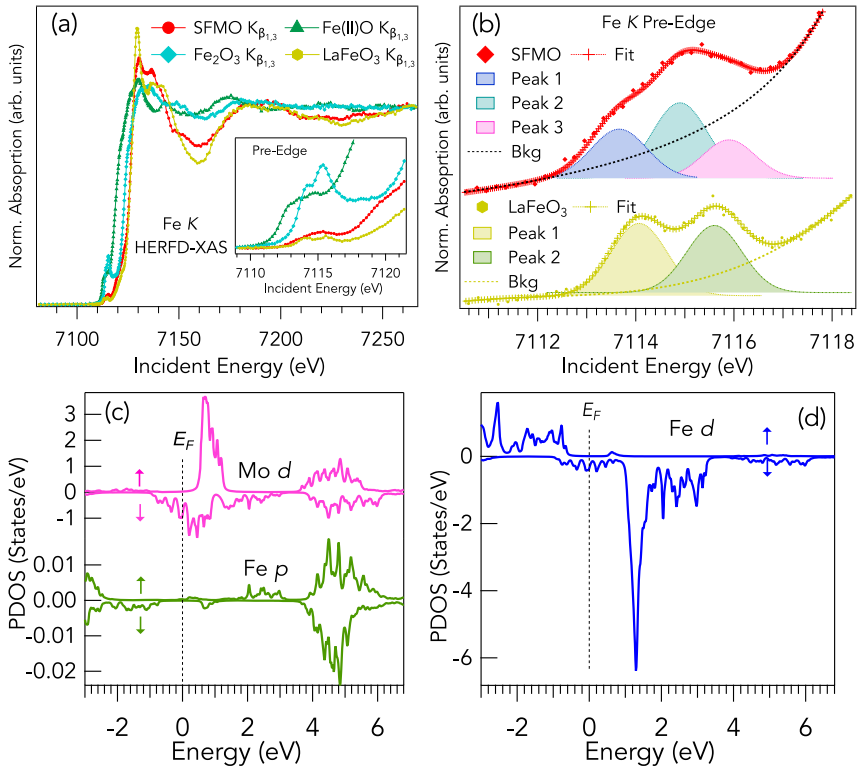

Figure 4. Fe K HERFD-XANES taken at the maximum of K$\beta_{1,3}$ X-ray emission peak for SFMO and related Fe oxides. Spectra are normalized to the K-edge jump at 7263 eV. (b) Fitting of pre-edge peaks for $LaFeO_3$ and SFMO. (c) Spin-resolved partial density of states (PDOS) of Fe p and Mo d orbitals and (d) Fe d PDOS. The Fermi level (E_F) is set at 0 eV and indicated by a dashed line.

(Fe^{2+}), Fe_3O_4, α-Fe_2O_3 (Fe^{3+}), and $LaFeO_3$ (Fe^{3+}). Although these references have different crystal structures, the local atomic coordination is also octahedral. We observe that the absorption edge shifts to higher energies for the Fe^{3+} compounds as expected and reported previously for Fe oxides.[40]

The pre-edge structure also evolves in spectral shape and intensity between Fe reference oxides and SFMO (Figure 4b inset). SFMO exhibits two main pre-edge structures centered near 7115 and 7120 eV. These features are attributed to quadrupolar (1s → 3d) and dipolar (1s → 4p) transitions, resulting in overlapping lines, and therefore single transitions cannot be easily distinguished. However, general trends can be observed based on the intensity and energy position. The first pre-edge feature is assigned to a 1s → 3d quadrupolar transition that is localized at the Fe absorbing atom.[41] More than one feature can be identified in this energy range because of the splitting of the 3d orbital energy levels. In the crystal-field picture, the quadrupolar prepeak intensity distribution change systematically with spin state, oxidation state, and local geometry.[42] Because of differences in crystallographic symmetry, it is only appropriate to compare the pre-edge of structures of $LaFeO_3$ and SFMO, as FeO and α-Fe_2O_3 assume rock-salt and corundum crystal structures, respectively. As shown in the bottom panel of Figure 3b, two well-resolved pre-edge features can be distinguished for $LaFeO_3$. They correspond to local quadrupolar 1s → 3d transition into unoccupied t_{2g} and e_g states, although they have been suggested to carry some O 2p character as reported in previous studies,[25,43,44] The splitting of the two pre-edge peaks for $LaFeO_3$ is 1.53 eV, which correspond to the crystal-field splitting of 1.50 eV as reported by Haas et al.[43] For SFMO, we find that three peaks are necessary for a reasonable fit of the Fe K pre-edge. The first two features, labeled Peaks 1 and 2 in Figure 3b, are separated by 1.23 eV and can be readily accounted as transitions to crystal field split t_{2g} and e_g states,

https://doi.org/10.1021/acs.jpcc.1c02580
J. Phys. Chem. C 2021, 125, 11249−11256

respectively, which is close to the crystal-field splitting of 1.25 eV from our calculations. The third pre-edge feature, centered at 7115.9 eV labeled Peak 3, is compatible with a mixture of quadrupolar and a dipolar transition that involve a neighboring Mo site.[41]

In transition metal oxides, dipolar contributions in the pre-edge can also arise from transitions to neighboring d states that are mediated via bridging oxygen through intersite Fe (4p)−O (2p)−Mo (4d)[25,41,45] hybridized states. Similar nonlocal features have also been identified in manganites[46] and cobaltites.[35,47] The strength of this nonlocal dipole contribution is primarily determined by the degree of covalency and thus by B−O bond lengths and the B−O−B′ bond angle which will influence the orbital overlap. Orthorhombic $LaFeO_3$ consists of corner-shared distorted octahedra[48] with a Fe−O−Fe bond angle values of 157°, while tetragonal SFMO consists of corner-shared octahedra[22] with Fe−O−Mo band angle closer to 180°. This near-collinear geometric arrangement maximizes the overlap to the 2p orbital of the bridging oxygen to make the most effective link and Fe 4p−O 2p−Mo 4d (unpublished results).[49] The Fe−O bond lengths in $LaFeO_3$ and SFMO are 1.988 and 1.985 Å, respectively, which suggests that the collinear structure bears more weight on the intensity of the nonlocal intersite pre-edge structure.

We support this interpretation by analyzing the calculated partial density of states (PDOS) that are separated into spin-up and spin-down contributions as shown in Figures 4c and 4d. The Fe d PDOS, shown in Figure 4d, shows a sizable intensity in the unoccupied region of the spin-down channel around 1 eV above the E_F that defines the local quadrupolar 1s → 3d transitions. The PDOS of Fe p orbitals furthermore shows structures for both spin directions at about 4.5 eV above the Fermi level, which could correspond to the absorption feature shown around 7120 eV. Similar structures are also observed in the PDOS of Mo d states at the same position of energy axis, implying hybridization between Mo d orbitals and Fe p orbitals. Moreover, the spin-down Fe d PDOS shows a relatively small intensity around 2 eV above E_F that most likely correspond to the "Peak 3" intrasite transition for SFMO with oxygen mediated intersite mixing between Fe p state and adjacent neighbor Mo d state. In fact, concomitant Fe p and Mo d (spin-down) DOS are present at the same energy. The small Fe PDOS character explains the relative enhanced absorption feature intensity.

Recent studies using hard X-ray photoemission have shown features in core-level spectra of transition metals oxides which are consistently explained in terms of well-screened peaks.[50,51] With its increased probe depth, HAXPES measurements show true bulk electronic structure and reveal satellite features and screening effects due to the large probing depth otherwise not straightforward from soft X-rays. The inclusion of additional nonlocal screening channels has been shown to be useful for understanding the 2p photoelectron spectra of NiO,[52] cuprates,[53] ruthenates,[54] and manganites.[55] Although there are several reports on the Fe 2p core levels for SFMO,[56,57] measurements at high X-ray photon energies have yet to be reported to the best of our knowledge, particularly for the description of local and nonlocal features. Figure 5a shows the Fe 2p hard X-ray photoemission spectra along with reference Fe oxides. The Fe^{3+} reference α-Fe_2O_3, $LaFeO_3$, and Ca_2FeReO_6 compounds show two main-line peaks that are due to spin−orbit split Fe 2p core levels. For each spin−orbit component, there are also high binding energy (E_B) satellite

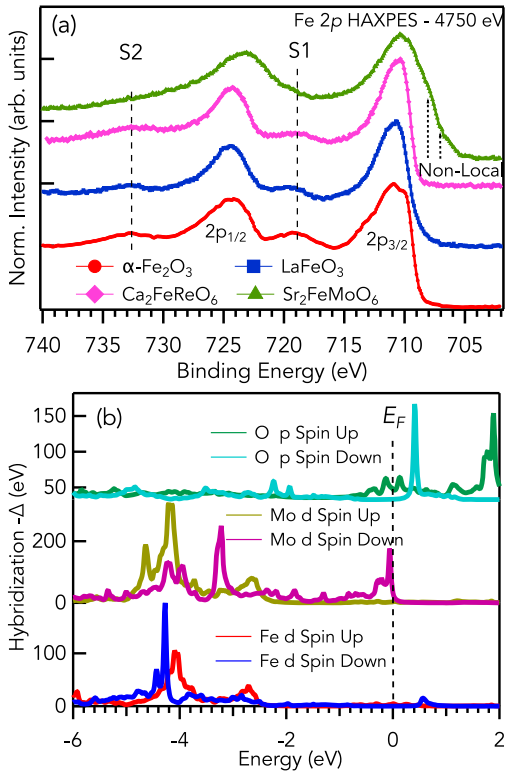

Figure 5. (a) Fe 2p HAXPES recorded with 4750 eV excitation energy for SFMO and several Fe^{3+} oxides. Spectra are normalized to the maximum of Fe $2p_{3/2}$ line. (b) Hybridization densities shown in a spin-resolved spectrum for Mo d, O p, and Fe d states.

features denoted as S1 and S2 in Figure 5a. These features have been previously assigned to charge-transfer (CT) structures that are dominated by $\underline{c}3d^5$ and $\underline{c}3d^6\underline{L}$ final states configurations,[58,59] where $\underline{c}$ and $\underline{L}$ denote a core hole and $\underline{L}$ a hole in the nearest ligand.

The SFMO Fe 2p HAXPES is characterized by broader main lines including a low binding energy contribution that are indicated by dashed arrows in Figure 5a. Low-E_B features in correlated oxides have varying explanations including a hole-doped bound state interaction like those in NiO,[52] a coherent metallic band formation in vanadates,[60] and magnetic transitions.[61] We exclude the broadening of the Fe 2p main line due to hole doping at the Fe site,[62,63] but rather due to the formation of a nonlocal metallic band with Mo 4d and O 2p character. This conclusion is supported from the hybridization function presented in Figure 5b, which shows very little contribution from Fe d states close to E_F. This observation is further corroborated by considering the asymmetric broadening of the O 1s photoemission line shape (see Figure S1b), which are common to systems with metallic screening.[64] The HAXPES binding energy position for SFMO O 1s is 529.1 eV, exactly matching the absorption threshold in the O 1s XAS spectrum of 529.0 eV, reflecting the empty oxygen 2p states at E_F. We therefore suggest that this line-shape change is due to delocalized states with considerable O 2p−Mo 4d hybridization. We exclude the lower binding energy features due to contributions from a lower valence such as Fe^{2+} or Fe^0, since the existence of such species would be detected with appreciable shifts from the measured Fe K absorption and emission spectra. Consequently, we attribute these low binding energy features at approximately 706 and 708 eV (indicated by

https://doi.org/10.1021/acs.jpcc.1c02580
J. Phys. Chem. C 2021, 125, 11249−11256

arrows in Figure 5a) to screening from hybridized Fe 3d−O 2p−Mo 4d valence states that screen the photoexcited Fe. From previously reported double cluster calculations on SFMO,[20] the ground state was reported to be described by a mixed character of ionic $3d^5$ as well as locally screened $3d^6\underline{L}$ and nonlocal $3d^6\underline{\nu}$ configurations, where $\underline{\nu}$ represent a hole in the valence band. The nonlocal screening involves an oxygen mediated Fe 3d−O 2p−Mo 4d hybridization. This configuration interaction picture has merit due to the strong nonlocal character of the ground state of SFMO.

Nonlocal screening has been successfully discussed in terms of the energy-dependent hybridization function in correlated systems.[51,65] The hybridization function encodes orbital and spin interactions and is composed of distance-shell contributions.[65,66] The larger the magnitude of hybridization function, the larger the overlap of that orbital with all other orbitals. The spin-resolved hybridization function is shown in Figure 5b. The intensities from 2 to −2 eV for Mo d corresponds to hybridized delocalized Mo 4d bands. The intensity is rather strong for Mo minority d states close to the E_F, largely attributable to the stronger amplitude of an indirect Fe−O−Mo hopping term, i.e., the conducting minority spin channel. This gives merit to a ground-state configuration with a hole in the valence band ($3d^6\underline{\nu}$) that tracks its origin to the spin-down Mo d band validating nonlocal effects in SFMO. We note that the hybridization function of Mo d majority states does not show any strong feature close to the Fermi level. The hybridization strength at E_F that are prominent for Mo d bands shown in Figure 5b are responsible for the width and shape of the Fe 2p low-E_B features. The hybridization function being the main indicator of itinerancy and localization, our results illustrate the significance of analyzing spin-resolved character of the Mo d bands for understanding the nonlocal effects in SFMO.

CONCLUSIONS

We have investigated the electronic structure properties of SFMO through several hard X-ray core-level spectroscopies. Our study provides direct support for nonlocal effects in SFMO. From Fe K-edge absorption and emission, we find that SFMO exhibits a high-spin $3d^5$ configuration with a nominal spin density of $S = 2.5$, similar to its trivalent Fe^{3+} analogues. Fe K-edge HERFD-XANES in SFMO shows a broad pre-edge structure that is a convolution of quadrupolar and dipolar peaks, one of which can be linked to an excitation in an intersite Fe 4p−O 2p−Mo 4d band. The spin-selective HERFD-XANES spectra show pre-edge features that are characteristics of spin-polarized properties of SFMO. Hard X-ray photoemission for the Fe 2p core-level show several structures in the low-E_B region that are highly probable of a nonlocal screening channel from an electron near the Fermi level. This nonlocal screening can effectively be tied to the strong hybridization density from the Mo 4d band, a consequence of optimal near-collinear Fe−O−Mo lattice geometry in SFMO. Our results point to a strong relationship between localized and nonlocalized character in SFMO that leads to its large T_C and high spin polarization. These results highlight the significance of nonlocal charge interactions in mediating a large exchange coupling strength (J) between Fe and Mo, where T_C is maximized. This combined approach of hard X-ray core-level spectroscopy techniques with theoretical simulations that include intersite effects is very useful to gain insights into double perovskite oxides and correlated systems in general. We hope our results advances the fundamental understanding of intersite physics in magnetic oxides that can lead to new directions in spintronic applications.

ASSOCIATED CONTENT

Supporting Information

The Supporting Information is available free of charge at https://pubs.acs.org/doi/10.1021/acs.jpcc.1c02580.

X-ray absorption spectroscopy taken at the O K-edge for SFMO and Fe reference compounds and O 1s hard X-ray photoemission spectra (PDF)

AUTHOR INFORMATION

Corresponding Authors

Dibya Phuyal − *Division of Molecular & Condensed Matter Physics, Department of Physics, Uppsala University, SE-75121 Uppsala, Sweden; Division of Material and Nano Physics, Department of Applied Physics, KTH Royal Institute of Technology, SE-106 91 Stockholm, Sweden;* orcid.org/0000-0003-0351-3138; Email: dibya@kth.se

Olof Karis − *Division of Molecular & Condensed Matter Physics, Department of Physics, Uppsala University, SE-75121 Uppsala, Sweden;* orcid.org/0000-0001-6406-217X; Email: olof.karis@physics.uu.se

Authors

Soham Mukherjee − *Division of Molecular & Condensed Matter Physics, Department of Physics, Uppsala University, SE-75121 Uppsala, Sweden*

Swarup K. Panda − *Department of Physics, Bennett University, Greater Noida 201310, Uttar Pradesh, India;* orcid.org/0000-0001-6675-3396

Gabriel J. Man − *Division of Molecular & Condensed Matter Physics, Department of Physics, Uppsala University, SE-75121 Uppsala, Sweden;* orcid.org/0000-0003-2932-7018

Konstantin Simonov − *Division of Molecular & Condensed Matter Physics, Department of Physics, Uppsala University, SE-75121 Uppsala, Sweden*

Laura Simonelli − *CELLS-ALBA Synchrotron, E-08290 Barcelona, Spain;* orcid.org/0000-0001-5331-0633

Sergei M. Butorin − *Division of Molecular & Condensed Matter Physics, Department of Physics, Uppsala University, SE-75121 Uppsala, Sweden;* orcid.org/0000-0003-3242-5305

Håkan Rensmo − *Division of Molecular & Condensed Matter Physics, Department of Physics, Uppsala University, SE-75121 Uppsala, Sweden*

Complete contact information is available at: https://pubs.acs.org/10.1021/acs.jpcc.1c02580

Notes

The authors declare no competing financial interest.

ACKNOWLEDGMENTS

We acknowledge CLAESS beamline at the ALBA Synchrotron, P22 beamline at DESY, and BL 8.0.1 at ALS for allocation of beamtime. This work was supported financially in part by the Swedish Research Council (Grants 2020-00681 and 2018-04330), the Swedish Energy Agency (Grant P43549-1), the Knut and Alice Wallenberg Foundation (2012.0031), and the Tryggers Foundation (Grant CTS-17:376).

■ ABBREVIATIONS

DP, double perovskite; TM, transition metal; SFMO, Sr_2FeMoO_6; XAS, X-ray absorption spectroscopy; XES, X-ray emission spectroscopy; HAXPES, hard X-ray photoemission spectroscopy; LDA, local density approximation; DMFT, dynamical mean-field theory; HERFD-XANES, high-resolution fluorescence detected X-ray absorption; TEY, total electron yield; TFY, total fluorescence yield; DFT, density functional theory; FP-LMTO, full potential linearized muffin-tin orbital method; BZ, Brillouin-zone; GGA+*U*, gradient approximation + Hubbard *U*; IAD, integral absolute difference; RXES, resonant X-ray emission; PDOS, partial density of states.

■ REFERENCES

(1) Vasala, S.; Karppinen, M. Progress in Solid State Chemistry A2B'B"O6 Perovskites: A Review. *Prog. Solid State Chem.* **2015**, *43*, 1−36.

(2) Martins, C.; Aichhorn, M.; Biermann, S. Coulomb Correlations in 4d and 5d Oxides from First Principles - Or How Spin-Orbit Materials Choose Their Effective Orbital Degeneracies. *J. Phys.: Condens. Matter* **2017**, *29*, 263001.

(3) Nechache, R.; Harnagea, C.; Li, S.; Cardenas, L.; Huang, W.; Chakrabartty, J.; Rosei, F. Bandgap Tuning of Multiferroic Oxide Solar Cells. *Nat. Photonics* **2015**, *9*, 61−67.

(4) Paul, A. K.; Reehuis, M.; Ksenofontov, V.; Yan, B.; Hoser, A.; Többens, D. M.; Abdala, P. M.; Adler, P.; Jansen, M.; Felser, C. Lattice Instability and Competing Spin Structures in the Double Perovskite Insulator Sr2FeOsO6. *Phys. Rev. Lett.* **2013**, *111*, 167205.

(5) Kobayashi, K.-I.; Kimura, T.; Tomioka, Y.; Sawada, H.; Terakura, K.; Tokura, Y. Intergrain Tunneling Magnetoresistance in Polycrystals of the Ordered Double Perovskite Sr2FeReO6. *Phys. Rev. B: Condens. Matter Mater. Phys.* **1999**, *59* (17), 11159−11162.

(6) Szotek, Z.; Temmerman, M.; Svane, A.; Petit, L.; Winter, H. Electronic Structure of Half-Metallic Double Perovskites. *Phys. Rev. B: Condens. Matter Mater. Phys.* **2003**, *68*, 104411.

(7) Erten, O.; Meetei, O. N.; Mukherjee, A.; Randeria, M.; Trivedi, N.; Woodward, P. Theory of Half-Metallic Ferrimagnetism in Double Perovskites. *Phys. Rev. Lett.* **2011**, *107*, 1−4.

(8) Suntivich, J.; May, K. J.; Gasteiger, H. A.; Goodenough, J. B.; Shao-Horn, Y. A Perovskite Oxide Optimized for Oxygen Evolution Catalysis from Molecular Orbital Principles. *Science* **2011**, *334* (6061), 1383−1385.

(9) Kobayashi, K. I.; Kimura, T.; Sawada, H.; Terakura, K.; Tokura, Y. Room-Temperature Magnetoresistance in an Oxide Material with an Ordered Double-Perovskite Structure. *Nature* **1998**, *395*, 677−680.

(10) Sarma, D. D.; Mahadevan, P.; Saha-Dasgupta, T.; Ray, S.; Kumar, A. Electronic Structure of Sr2FeMoO6. *Phys. Rev. Lett.* **2000**, *85*, 2549−2552.

(11) Ray, S.; Kumar, A.; Sarma, D. D.; Cimino, R.; Turchini, S.; Zennaro, S.; Zema, N. Electronic and Magnetic Structures of Sr2FeMoO6. *Phys. Rev. Lett.* **2001**, *87*, No. 097204.

(12) Bibes, M.; Bouzehouane, K.; Barthélémy, A.; Besse, M.; Fusil, S.; Bowen, M.; Seneor, P.; Carrey, J.; Cros, V.; Vaurès, A.; et al. Tunnel Magnetoresistance in Nanojunctions Based on Sr2FeMoO6. *Appl. Phys. Lett.* **2003**, *83*, 2629.

(13) García-Landa, B.; Ritter, C.; Ibarra, M. R.; Blasco, J.; Algarabel, P. A.; Mahendiran, R.; García, J. Magnetic and Magnetotransport Properties of the Ordered Perovskite Sr2FeMoO6. *Solid State Commun.* **1999**, *110*, 435−438.

(14) Saloaro, M.; Hoffmann, M.; Adeagbo, W. A.; Granroth, S.; Deniz, H.; Palonen, H.; Huhtinen, H.; Majumdar, S.; Laukkanen, P.; Hergert, W.; et al. Toward Versatile Sr2FeMoO6 Based Spintronics by Exploiting Nanoscale Defects. *ACS Appl. Mater. Interfaces* **2016**, *8*, 20440−20447.

(15) Serrate, D.; De Teresa, J. M.; Ibarra, M. R. Double Perovskites with Ferromagnetism above Room Temperature. *J. Phys.: Condens. Matter* **2007**, *19*, No. 023201.

(16) Estrada, F.; Guzmán, E. J.; Navarro, O.; Avignon, M. Curie Temperature Behavior in Half-Metallic Ferromagnetic Double Perovskites within the Electronic Correlation Picture. *Phys. Rev. B: Condens. Matter Mater. Phys.* **2018**, *97*, 195155.

(17) Tomioka, Y.; Okuda, T.; Okimoto, Y.; Kumai, R.; Kobayashi, K.; Tokura, Y. Magnetic and Electronic Properties of a Single Crystal of Ordered Double Perovskite Sr2FeMoO6. *Phys. Rev. B: Condens. Matter Mater. Phys.* **2000**, *61*, 422−427.

(18) Saha-Dasgupta, T.; Sarma, D. D. Ab Initio Study of Disorder Effects on the Electronic and Magnetic Structure of Sr2FeMoO6. *Phys. Rev. B: Condens. Matter Mater. Phys.* **2001**, *64*, No. 064408.

(19) Brey, L.; Calderón, M. J.; Das Sarma, S.; Guinea, F. Mean-Field Theory for Double Perovskites: Coupling between Itinerant Electron Spins and Localized Spins. *Phys. Rev. B: Condens. Matter Mater. Phys.* **2006**, *74*, No. 094429.

(20) Martins, H. P.; Guedes, E. B.; Mossanek, R. J. O.; Prado, F. D.; Caneiro, A.; Abbate, M. Many-Body Effects and Non-Local Charge Fluctuations in the Double Perovskite Sr2FeMoO6. *RSC Adv.* **2018**, *8*, 3928−3933.

(21) De Groot, F. M. F.; Kotani, A. *Core Level Spectroscopy of Solids*; CRC Press: Boca Raton, FL, 2008.

(22) Jana, S.; Meneghini, C.; Sanyal, P.; Sarkar, S.; Saha-Dasgupta, T.; Karis, O.; Ray, S. Signature of an Antiferromagnetic Metallic Ground State in Heavily Electron-Doped Sr2FeMoO6. *Phys. Rev. B: Condens. Matter Mater. Phys.* **2012**, *86*, No. 054433.

(23) Kato, H.; Okuda, T.; Okimoto, Y.; Tomioka, Y.; Oikawa, K.; Kamiyama, T.; Tokura, Y. Metal-Insulator Transition of Ferromagnetic Ordered Double Perovskites: (Sr1-YCay)2FeReO6. *Phys. Rev. B: Condens. Matter Mater. Phys.* **2002**, *65*, 144404.

(24) Simonelli, L.; Marini, C.; Olszewski, W.; Ávila Pérez, M.; Ramanan, N.; Guilera, G.; Cuartero, V.; Klementiev, K. CLÆSS: The Hard X-Ray Absorption Beamline of the ALBA CELLS Synchrotron. *Cogent Phys.* **2016**, *3*, 1−10.

(25) Glatzel, P.; Mirone, A.; Eeckhout, S. G.; Sikora, M.; Giuli, G. Orbital Hybridization and Spin Polarization in the Resonant 1s Photoexcitations of α-Fe_2O_3. *Phys. Rev. B: Condens. Matter Mater. Phys.* **2008**, *77*, 115133.

(26) Qiao, R.; Li, Q.; Zhuo, Z.; Sallis, S.; Fuchs, O.; Blum, M.; Weinhardt, L.; Heske, C.; Pepper, J.; Jones, M.; et al. High-Efficiency in Situ Resonant Inelastic x-Ray Scattering (IRIXS) Endstation at the Advanced Light Source. *Rev. Sci. Instrum.* **2017**, *88*, No. 033106.

(27) Schlueter, C.; Gloskovskii, A.; Ederer, K.; Schostak, I.; Piec, S.; Sarkar, I.; Matveyev, Y.; Lömker, P.; Sing, M.; Claessen, R.; et al. The New Dedicated HAXPES Beamline P22 at PETRAIII. In *AIP Conference Proceedings*; 2019; p 040010.

(28) Andersen, O. K. Linear Methods in Band Theory. *Phys. Rev. B* **1975**, *12*, 3060.

(29) Wills, J. M.; Cooper, B. R. Synthesis of Band and Model Hamiltonian Theory for Hybridizing Cerium Systems. *Phys. Rev. B: Condens. Matter Mater. Phys.* **1987**, *36*, 3809.

(30) Wills, J. M., Eriksson, O., Alouani, M., Price, D. L. *Electronic Structure and Physical Properties of Solids: The Uses of the LMTO Method*; Dreysse, H., Ed.; Springer-Verlag: Berlin, 2000.

(31) Samanta, S.; Mishra, S. B.; Nanda, B. R. K. Quantum Well Structure of a Double Perovskite Superlattice and Formation of a Spin-Polarized Two-Dimensional Electron Gas. *Phys. Rev. B: Condens. Matter Mater. Phys.* **2018**, *98*, 115155.

(32) Rovezzi, M.; Glatzel, P. Hard X-Ray Emission Spectroscopy: A Powerful Tool for the Characterization of Magnetic Semiconductors. *Semicond. Sci. Technol.* **2014**, *29*, No. 023002.

(33) Lafuerza, S.; Carlantuono, A.; Retegan, M.; Glatzel, P. Chemical Sensitivity of Kβ and Kα X-Ray Emission from a Systematic Investigation of Iron Compounds. *Inorg. Chem.* **2020**, *59*, 12518−12535.

(34) Vankó, G.; Neisius, T.; Molnár, G.; Renz, F.; Kárpáti, S.; Shukla, A.; De Groot, F. M. F. Probing the 3D Spin Momentum with

https://doi.org/10.1021/acs.jpcc.1c02580
J. Phys. Chem. C 2021, 125, 11249−11256

X-Ray Emission Spectroscopy: The Case of Molecular-Spin Transitions. *J. Phys. Chem. B* **2006**, *110*, 11647−11653.
(35) Lafuerza, S.; García, J.; Subías, G.; Blasco, J.; Glatzel, P. High-Resolution Mn K-Edge x-Ray Emission and Absorption Spectroscopy Study of the Electronic and Local Structure of the Three Different Phases in Nd0.5Sr0.5MnO3. *Phys. Rev. B: Condens. Matter Mater. Phys.* **2016**, *93*, 31−33.
(36) Peng, G.; deGroot, F. M. F.; Haemaelaeinen, K.; Moore, J. A.; Wang, X.; Grush, M. M.; Hastings, J. B.; Siddons, D. P.; Armstrong, W. H. High-Resolution Manganese x-Ray Fluorescence Spectroscopy. Oxidation-State and Spin-State Sensitivity. *J. Am. Chem. Soc.* **1994**, *116*, 2914−2920.
(37) Hayashi, H.; Sato, A.; Azumi, T.; Udagawa, Y.; Inami, T.; Ishii, K.; Garg, K. B. Local Spin Ordering in the Antiferromagnetic as Well as Paramagnetic LaMnO3 Phase Revealed by Polarized Spin-Selected 1s-3d Absorption Spectra. *Phys. Rev. B: Condens. Matter Mater. Phys.* **2006**, *73*, 134405.
(38) De Groot, F. M. F.; Pizzini, S.; Fontaine, A.; Hämäläinen, K.; Kao, C. C.; Hastings, J. B. Local-Spin-Selective x-Ray Absorption and x-Ray Magnetic Circular Dichroism of Mn. *Phys. Rev. B: Condens. Matter Mater. Phys.* **1995**, *51* (2), 1045−1052.
(39) Hämäläinen, K.; Siddons, D. P.; Hastings, J. B.; Berman, L. E. Elimination of the Inner-Shell Lifetime Broadening in x-Ray-Absorption Spectroscopy. *Phys. Rev. Lett.* **1991**, *67*, 2850−2853.
(40) De Groot, F. M. F.; Glatzel, P.; Bergmann, U.; Van Aken, P. A.; Barrea, R. A.; Klemme, S.; Hävecker, M.; Knop-Gericke, A.; Heijboer, W. M.; Weckhuysen, B. M. 1s2p Resonant Inelastic X-Ray Scattering of Iron Oxides. *J. Phys. Chem. B* **2005**, *109*, 20751−20762.
(41) De Groot, F.; Vankó, G.; Glatzel, P. The 1s X-Ray Absorption Pre-Edge Structures in Transition Metal Oxides. *J. Phys.: Condens. Matter* **2009**, *21*, 104207.
(42) Westre, T. E.; Kennepohl, P.; DeWitt, J. G.; Hedman, B.; Hodgson, K. O.; Solomon, E. I. A Multiplet Analysis of Fe K-Edge $1\vec{s}$ 3d Pre-Edge Features of Iron Complexes. *J. Am. Chem. Soc.* **1997**, *119*, 6297−6314.
(43) Haas, O.; Vogt, U. F.; Soltmann, C.; Braun, A.; Yoon, W. S.; Yang, X. Q.; Graule, T. The Fe K-Edge X-Ray Absorption Characteristics of La1-XSrxFeO3-δ Prepared by Solid State Reaction. *Mater. Res. Bull.* **2009**, *44*, 1397−1404.
(44) Glatzel, P.; Bergmann, U. High Resolution 1s Core Hole X-Ray Spectroscopy in 3d Transition Metal Complexes - Electronic and Structural Information. *Coord. Chem. Rev.* **2005**, *249*, 65−95.
(45) Glatzel, P.; Sikora, M.; Fernández-García, M. Resonant X-Ray Spectroscopy to Study K Absorption Pre-Edges in 3d Transition Metal Compounds. *Eur. Phys. J.: Spec. Top.* **2009**, *169*, 207−214.
(46) Rybicki, D.; Sikora, M.; Przewoznik, J.; Kapusta, C.; Mitchell, J. F. Interplay of Local Structure, Charge, and Spin in Bilayered Manganese Perovskites. *Phys. Rev. B: Condens. Matter Mater. Phys.* **2018**, *97*, 115158.
(47) Cuartero, V.; Lafuerza, S.; Rovezzi, M.; García, J.; Blasco, J.; Subías, G.; Jiménez, E. X-Ray Absorption and Emission Spectroscopy Study of Mn and Co Valence and Spin States in TbMn1−xCoxO3. *Phys. Rev. B: Condens. Matter Mater. Phys.* **2016**, *94*, 155117.
(48) Phuyal, D.; Mukherjee, S.; Panda, S. K.; Jana, S.; Segre, C. U.; Simonelli, L.; Butorin, S. M.; Rensmo, H.; Karis, O. Origin of Itinerant Carriers in Antiferromagnetic LaFe1-XMoxO3 Studied by X-Ray Spectroscopies. *Phys. Rev. Mater.* **2020**, *4*, No. 034405.
(49) Vankó, G.; de Groot, F. M. F.; Huotari, S.; Cava, R. J.; Lorenz, T.; Reuther, M. *Intersite 4p-3d Hybridization in Cobalt Oxides: A Resonant X-Ray Emission Spectroscopy Study*, 2008.
(50) Taguchi, M.; Chainani, A.; Kamakura, N.; Horiba, K.; Takata, Y.; Yabashi, M.; Tamasaku, K.; Nishino, Y.; Miwa, D.; Ishikawa, T.; et al. Bulk Screening in Core-Level Photoemission from Mott-Hubbard and Charge-Transfer Systems. *Phys. Rev. B: Condens. Matter Mater. Phys.* **2007**, *76*, 169901.
(51) Horiba, K.; Taguchi, M.; Chainani, A.; Takata, Y.; Ikenaga, E.; Miwa, D.; Nishino, Y.; Tamasaku, K.; Awaji, M.; Takeuchi, A.; et al. Nature of the Well Screened State in Hard X-Ray Mn 2p Core-Level Photoemission Measurements of La1-XSrxMnO3 Films. *Phys. Rev. Lett.* **2004**, *93*, 236401.
(52) Taguchi, M.; Matsunami, M.; Ishida, Y.; Eguchi, R.; Chainani, A.; Takata, Y.; Yabashi, M.; Tamasaku, K.; Nishino, Y.; Ishikawa, T.; et al. Revisiting the Valence-Band and Core-Level Photoemission Spectra of NiO. *Phys. Rev. Lett.* **2008**, *100*, 206401.
(53) Van Veenendaal, M. Competition between Screening Channels in Core-Level x-Ray Photoemission as a Probe of Changes in the Ground-State Properties of Transition-Metal Compounds. *Phys. Rev. B: Condens. Matter Mater. Phys.* **2006**, *74* (8), No. 085118.
(54) Guedes, E. B.; Abud, F.; Martins, H. P.; Abbate, M.; Jardim, R. F.; Mossanek, R. J. O. Role of Ti-Ru Interaction in SrTi0.5Ru0.5O3: Physical Properties, x-Ray Spectroscopy, and Cluster Model Calculations. *Phys. Rev. B: Condens. Matter Mater. Phys.* **2019**, *100*, No. 075132.
(55) Hariki, A.; Yamanaka, A.; Uozumi, T. Orbital- and Spin-Order Sensitive Nonlocal Screening in Mn 2p X-Ray Photoemission of La1-XSrxMnO3. *EPL* **2016**, *114*, 27003.
(56) Kim, J. H.; Wi, S. C.; Yoon, S.; Suh, B. J.; Han, S. W.; Kim, K. H.; Sekiyama, A.; Kasai, S.; Suga, S.; Hwang, C.; et al. Photoemission and X-Ray Absorption Spectroscopy Study of Magnetoresistive Double Perovskite Oxides. *J. Korean Phys. Soc.* **2003**, *43* (3), 416−422.
(57) Jalili, H.; Heinig, N. F.; Leung, K. T. X-Ray Photoemission Study of Sr2FeMoO6 and SrMoO4 Films Epitaxially Grown on MgO(001): Near-Surface Chemical-State Composition Analysis. *Phys. Rev. B: Condens. Matter Mater. Phys.* **2009**, *79*, 174427.
(58) Miedema, P. S.; Borgatti, F.; Offi, F.; Panaccione, G.; De Groot, F. M. F. Iron 1s X-Ray Photoemission of Fe_2O_3. *J. Electron Spectrosc. Relat. Phenom.* **2015**, *203*, 8−13.
(59) Wang, L.; Du, Y.; Sushko, P. V.; Bowden, M. E.; Stoerzinger, K. A.; Heald, S. M.; Scafetta, M. D.; Kaspar, T. C.; Chambers, S. A. Hole-Induced Electronic and Optical Transitions in La1-XSrxFeO3 Epitaxial Thin Films. *Phys. Rev. Mater.* **2019**, *3*, No. 025401.
(60) Eguchi, R.; Taguchi, M.; Matsunami, M.; Horiba, K.; Yamamoto, K.; Ishida, Y.; Chainani, A.; Takata, Y.; Yabashi, M.; Miwa, D.; et al. Photoemission Evidence for a Mott-Hubbard Metal-Insulator Transition in VO2. *Phys. Rev. B: Condens. Matter Mater. Phys.* **2008**, *78*, No. 075115.
(61) Gatti, M.; Panaccione, G.; Reining, L. Effects of Low-Energy Excitations on Spectral Properties at Higher Binding Energy: The Metal-Insulator Transition of VO2. *Phys. Rev. Lett.* **2015**, *114*, 116402.
(62) Frati, F.; Hunault, M. O. J. Y.; De Groot, F. M. F. Oxygen K-Edge X-Ray Absorption Spectra. *Chem. Rev.* **2020**, *120*, 4056−4110.
(63) Chen, C. T.; Sette, F.; Ma, Y.; Hybertsen, M. S.; Stechel, E. B.; Foulkes, W. M. C.; Schulter, M.; Cheong, S. W.; Cooper, A. S.; Rupp, L. W.; et al. Electronic States in La2-XSrxCuO4+ Probed by Soft x-Ray Absorption. *Phys. Rev. Lett.* **1991**, *66*, 104.
(64) Woicik, J. C. *Hard X-Ray Photoelectron Spectroscopy (HAXPES)*; Woicik, J. C., Ed.; Springer International Publishing AG: Heidelberg, 2016.
(65) Ghiasi, M.; Hariki, A.; Winder, M.; Kuneš, J.; Regoutz, A.; Lee, T. L.; Hu, Y.; Rueff, J. P.; De Groot, F. M. F. Charge-Transfer Effect in Hard x-Ray 1s and 2p Photoemission Spectra: LDA+DMFT and Cluster-Model Analysis. *Phys. Rev. B: Condens. Matter Mater. Phys.* **2019**, *100*, 75146.
(66) Hariki, A.; Uozumi, T.; Kuněs, J. LDA+DMFT Approach to Core-Level Spectroscopy: Application to 3d Transition Metal Compounds. *Phys. Rev. B: Condens. Matter Mater. Phys.* **2017**, *96*, 045111.

https://doi.org/10.1021/acs.jpcc.1c02580
J. Phys. Chem. C 2021, 125, 11249−11256